

## Numerical study of the flow of FENE-CR viscoelastic fluids in a planar cross-slot geometry

G.N. Rocha<sup>1</sup>, R.J. Poole<sup>2</sup>, M.A. Alves<sup>3</sup> and P.J. Oliveira<sup>1</sup>

<sup>1</sup> Universidade da Beira Interior, Departamento de Engenharia Electromecânica, Calçada Fonte do Lameiro,  
6201-001 Covilhã, Covilhã, Portugal

email: gerardorocha@portugalmail.pt, pipo@ubi.pt

<sup>2</sup> University of Liverpool, Department of Engineering, Brownlow Street, L69 3GH, Liverpool, United Kingdom  
email: robpoole@liverpool.ac.uk

<sup>3</sup> Faculdade de Engenharia da Universidade do Porto, Departamento de Engenharia Química, CEFT, Rua Dr.  
Roberto Frias, 4200-465 Porto, Porto, Portugal  
email: mmalves@fe.up.pt

---

### Abstract

*In order to understand the conditions for the onset of purely-elastic instabilities occurring in creeping flows ( $Re \approx 0$ ) of viscoelastic fluids we have carried out a systematic set of simulations in a planar cross-slot geometry governed by the non-linear constitutive equation FENE-CR. A finite-volume method is used for the calculation of the governing equations. Flow streamlines in the central region of the cross-slot become asymmetric above a critical Deborah number in agreement with experimental results and previously published results for infinite extensibility models (UCM and Oldroyd-B) [Phys. Rev. Lett. **99** 164503 (2007)].*

---

**Key Words:** Purely-elastic instabilities; Cross-slot geometry; Finite-volume method; Viscoelastic fluid; FENE-CR model.

### 1 Introduction

The motion of a viscoelastic fluid through a cross-slot device at low Reynolds number is one of the typical problems in non-Newtonian fluid mechanics: it allows very high extensional strains to be attained and it is prone to instabilities. In the past, Larson *et al.* [1] investigated numerically and experimentally the purely-elastic instabilities which occur in a Taylor-Couette flow of dilute polymer solutions. Recent studies of viscoelastic flows through cross-slot geometries have been conducted by Arratia *et al.* [2] and Poole *et al.* [3]. Arratia *et al.* [2] have reported two new flow instabilities in a micro-fabricated cross-slot geometry. In the first instability the flow becomes deformed and asymmetric, but remains steady. The second instability occurs at higher strain rates and leads to a velocity field fluctuating non-periodically in time. Later, Poole *et al.* [3] have shown, using a finite-volume method, that the steady asymmetric flow pattern can be predicted using the simplest differential viscoelastic model, the upper-convected Maxwell (UCM) model, at a negligible Reynolds number ( $Re = 0$ , i.e. in absence of inertial effects). At low Deborah numbers the flow remains steady and symmetric, whereas above a critical Deborah number ( $De_{cr} = 0.31$ ) the flow becomes asymmetric and steady. The findings of Poole *et al.* [3] have been a stimulus to further numerical studies, using more realistic FENE-type models [4] (Finitely Extensibility Nonlinear Elastic).

In addition to the occurrence of instabilities the calculation of steady viscoelastic flow through a cross-slot geometry has been the focus of attention for two reasons. First, it is important to be able to predict experimentally relevant flows which are dominated by extensional effects. Second, this problem has the potential of becoming a benchmark problem in computational rheology [3] for the comparison of results obtained with different numerical techniques.

In this paper we also demonstrate that the flow of a viscoelastic fluid obeying a non-linear constitutive equation becomes deformed and asymmetric, in the planar cross-slot geometry, above a critical Deborah number. To describe the rheology of the fluid we use the FENE-CR constitutive equation proposed by Chilcott and Rallison [5] and for solving the governing equations we apply a fully implicit finite-volume numerical method. The purpose of the present work is to provide quantitative data of benchmark quality for the cross-slot flow and explore the effects of finite extensibility. In Section 2, we present the governing equations, which are solved with the numerical method briefly explained in Section 3. The problem description and computational mesh are given

in Section 4, the results and discussions are presented in Section 5 and some conclusions are provided in Section 6.

## 2 Governing equations

The basic equations for two-dimensional (2-D), incompressible and isothermal, laminar flow of a viscoelastic FENE-CR fluid are the continuity equation:

$$\frac{\partial u_i}{\partial x_i} = 0 \quad (1)$$

the momentum conservation equation:

$$\rho \frac{\partial u_i}{\partial t} + \rho \frac{\partial u_i u_j}{\partial x_j} = -\frac{\partial p}{\partial x_i} + \frac{\partial \tau_{ij\text{tot}}}{\partial x_j} \quad (2)$$

and the rheological constitutive model equation:

$$\tau_{ij\text{tot}} = \eta_s \left( \frac{\partial u_i}{\partial x_j} + \frac{\partial u_j}{\partial x_i} \right) + \tau_{ij} \quad (3)$$

$$\tau_{ij} + \lambda \left( \frac{1}{f} \left[ \left( \frac{\partial \tau_{ij}}{\partial t} + u_k \frac{\partial \tau_{ij}}{\partial x_k} \right) - \tau_{ik} \frac{\partial u_j}{\partial x_k} - \tau_{jk} \frac{\partial u_i}{\partial x_k} \right] + \tau_{ij} \left( \frac{\partial \left( \frac{1}{f} \right)}{\partial t} + u_k \frac{\partial \left( \frac{1}{f} \right)}{\partial x_k} \right) \right) = \eta_p \left( \frac{\partial u_i}{\partial x_j} + \frac{\partial u_j}{\partial x_i} \right) \quad (4)$$

The function  $f(\tau)$  is expressed by:

$$f(\tau) = \frac{L^2 + (\lambda/\eta_p)(\tau_{kk})}{L^2 - 3} \quad (5)$$

where Einstein's summation convention is applied in all equations,  $\rho$  is the fluid density (assumed constant),  $p$  the pressure,  $u_i$  the velocity component along the Cartesian directions  $x_i$  ( $i = x, y$ ),  $\lambda$  the constant zero-shear rate relaxation time,  $\eta_s$  the solvent viscosity,  $\eta_p$  the contribution of the polymer to the total shear viscosity  $\eta_0 = \eta_s + \eta_p$  (also taken as constant) and  $L^2$  the extensibility parameter that measures the size of the polymer molecule in relation to its equilibrium size.

The relevant dimensionless parameters in this work are:

- $L^2$  – the extensibility parameter of FENE-CR model;
- $\beta = \eta_s/\eta_0$  – the solvent viscosity ratio;
- $Re = \rho U d / \eta_0$  – the Reynolds number;
- $De = \lambda U / d$  – the Deborah number.

## 3 Numerical method (discretization)

The equations of the previous section are transformed into a general non-orthogonal coordinate system for easy application of the finite-volume method (FVM) on a collocated mesh arrangement (see Fig. 1(a)). This method has become popular in Computational Fluid Dynamics (CFD) because it ensures that the discretization is conservative, i.e. mass and momentum are conserved over the whole domain. The governing equations (Eqs. (1) - (5)) are discretised by integration in space over the set of control volumes (cells, with volume  $V_p$ ) forming the computational mesh, and in time over a small time step,  $\delta t$ . This process results in systems of linearised algebraic equations for the equations of mass and momentum conservation jointly with the constitutive equation. In these equations all variables are evaluated and stored at the centre of each control volume (cells), as represented schematically in Fig. 1(b). As a consequence, special procedures are required to ensure the pressure/velocity coupling (following the Rhie and Chow method [6]) and the velocity/stress coupling (following Oliveira *et al.* approach [7]).

The discretised equation for the mass conservation Eq. (1) is written as:

$$\sum_f F_f = 0 \quad (6)$$

where  $F_f$  is the mass flux across cell face  $f$  (in this work  $f$  is varied from 1 to 4, for  $w, e, s$ , and  $n$  with compass notation: west, east, south and north, see Fig. 1(b)).

The linearised algebraic equation corresponding to the momentum conservation is expressed by:

$$a_p u_{i,P} = \sum_F a_F u_{i,F} + S_p(\nabla p) + S_{HRS}(u_i) + S_{Diffusion}(u_i) + S_\tau(\tau_{ij}) + \frac{\rho V_P}{\delta t} u_{i,P}^n \quad (7)$$

where  $a_p$  and  $a_F$  are the coefficients (accounting for convective and diffusive influences) and  $S$  terms (on the right hand side of Eq. (7)) represent the effects due to the pressure gradient, the high-resolution scheme, the artificial diffusive term (explicit part), and the elastic stress divergence term, respectively. The last term is the inertial term resulting from the temporal derivative of the momentum conservation. The index  $P$  denotes the cell at the centre of the computational mesh and  $F$  the corresponding neighbouring cells. The time-dependent terms in equations Eqs. (7) and (8) are retained in the discretization equations so that a steady-state solution is effectively approached by a succession of time advancement steps.

The discretised constitutive equation has the same form of the Eq. (7) and is represented by:

$$a_p^\tau \tau_{ij,P} = \sum_F a_F^\tau \tau_{ij,F} + S^\tau(\tau_{ij}, \nabla u_i) + S_{HRS}^\tau(\tau_{ij}) + \frac{\lambda_p V_P}{f(\tau_p) \delta t} \tau_{ij,P}^n \quad (8)$$

The difference between this equation and Eq. (7) is that the coefficients  $a_p^\tau$  and  $a_F^\tau$  only contain convective effects and there exists a new source term which depends simultaneously on the stress tensor and velocity gradients. In general, the coefficients of the discretised equations are calculated using the upwind scheme. For the calculation of convective terms we use a high-resolution scheme called CUBISTA [8] which is implemented explicitly through the deferred correction technique developed by Khosla and Rubin [9].

The continuity and momentum conservation equations in discretised form are solved using a semi-implicit method for pressure-linked equations proposed by Van Doormal and Raithby [10]. This method was based on the algorithm SIMPLE of Patankar and Spalding [11] which allows velocity and pressure fields to be obtained whilst simultaneously verifying the continuity and momentum equations. Two new steps are introduced in the initial part of the algorithm to account for the stress equation, as explained in more detail in Oliveira *et al.* [7].

The main steps of the present algorithm are as follows:

- Step 1:** In the first step of the algorithm the linear equations (Eq. (8)) for the stress tensor are solved sequentially, by a bi-conjugate gradient method, to obtain each stress component  $\tau_{ij}$  (velocity field from the previous time step).
- Step 2:** With updated stress fields obtained in the previous step, the discretised momentum conservation equations (Eq. (7)) are solved sequentially with the same method for each velocity component ( $u$  and  $v$ ), with an assumed pressure (from the previous time step).
- Step 3:** Finally, the discretised continuity equation (Eq. (6)) is rearranged into a Poisson pressure-correction equation which is implicitly solved for the pressure correction  $p'$  with a symmetric conjugate gradient. This is then added to the pressure from the previous time step and is also used to correct the velocity in order to satisfy continuity.

With the new values of  $\tau_{ij}$ ,  $u_i$  and  $p$ , the whole procedure can then be restarted at the new time level and repeated until the norm of the residuals of all equations becomes smaller than the prescribed tolerance (TOL). In this work we used  $TOL = 10^{-4}$ , based on normalised values, and it has been confirmed from numerical simulations that this tolerance provides an adequately converged solution. When all residuals were below  $10^{-4}$ , none of those six dependent variables (in this two-dimensional problem) were seen to vary significantly.

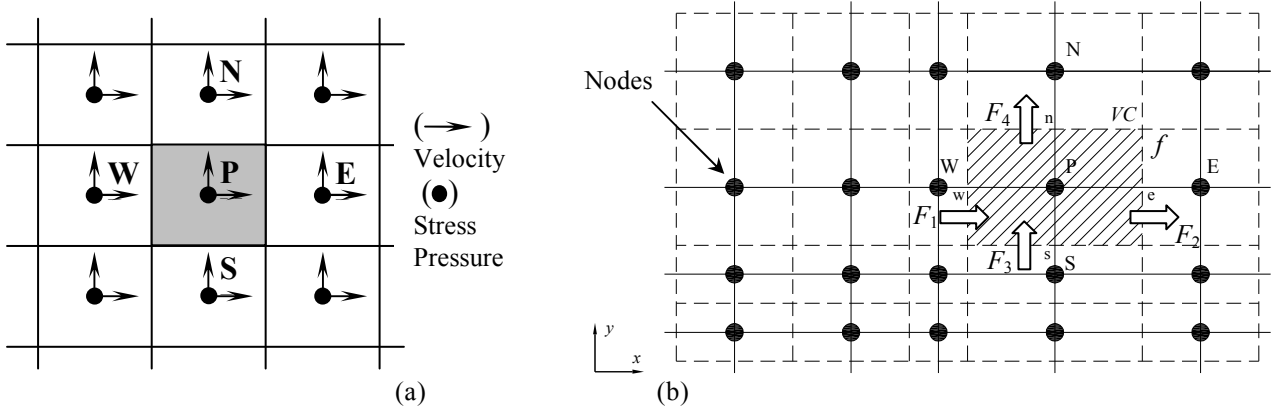


**Fig.1.** (a) Non-staggered mesh arrangement with all variables stored at the centre of cells. (b) Main control volume in a non-uniform mesh.

#### 4 Problem description and computational mesh

We consider the planar cross-slot geometry shown schematically in Fig. 2. Flow enters from left and right and leaves from top and bottom channels, with widths  $d$  and lengths  $10d$ . The top and bottom channel lengths are sufficient long for the outlet flow to become fully-developed and to avoid any effect of the outlet condition upon the flow in the central region of the cross-slot. For a Newtonian and viscoelastic flow, two incoming streams ( $Q$ ) meet at the intersection of the cross-slot and each of them divide in two streams ( $Q_1$  and  $Q_2$ ) and go into the top and bottom channels, generating a stagnation point ( $u = v = 0$ ) at the central position of the cross slot ( $x = 0, y = 0$ ), thus creating purely compressive and extensional flows near the central square.

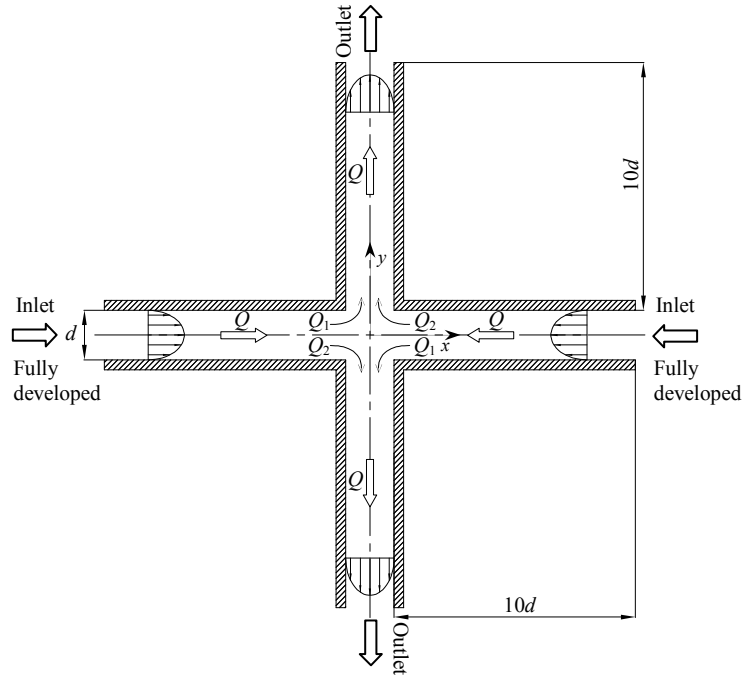


**Fig.2.** Schematic of the cross-slot flow geometry.

Boundary conditions are required for the dependent variables at the boundary faces of computational domain:

- Inlet ( $x = \pm 10.5d$ ): Fully developed velocity (average value  $U$ ) and stress profiles are imposed from analytical solutions.
- Outlet ( $y = \pm 10.5d$ ): Neumann's condition are applied to all variables ( $\psi$ ) i.e.  $\partial\psi/\partial y = 0$ , except the pressure which was linearly extrapolated from the inside channel.
- Wall ( $x = y = \pm 0.5d$ ): The no-slip condition applies to all the velocity components ( $u = v = 0$ ) with stress obtained from analytical expressions and pressure linearly extrapolated from two nearest neighbour cells (see [7]).

All the calculations were carried out for the limiting case of  $Re = 0$  and this was imposed in the computational code by equating the convective terms of the momentum equation to zero. A constant time step of  $\delta t = 0.01d/U$  was used in all calculations for the various Deborah numbers considered.

The 2-D geometry was divided into five blocks used to generate the computational mesh (see Fig. 3(a)), with blocks I and V in the inlet channels, III and IV in the outlet channels and II in the central region. The cells were made smaller along the inlet and outlet channels until the central square, using appropriate expansion or compression geometrical factors. In the central square ( $|x|$  and  $|y| \leq 1$ ) we have a uniform mesh with cell spacing  $\Delta x_{\min} \approx \Delta y_{\min} \approx 0.02d$ . This 2-D mesh has a total of 12801 cells which results in 76806 degrees-of-freedom. A summary of the main characteristics of the computational mesh is presented in Table 1. The Table includes the number of control volumes (or cells),  $N_x$  along the  $x$ -direction,  $N_y$  along the  $y$ -direction, and the expansion or compression geometrical factors for each  $x$  and  $y$  directions.

**Table 1.** Main characteristics of computational mesh.

Blocks	$N_x$	$N_y$	$f_x$	$f_y$
I	50	51	0.929296	1.000000
II	51	51	1.000000	1.000000
III	51	50	1.000000	0.929296
IV	51	50	1.000000	1.075369
V	50	51	1.075369	1.000000
NC <sup>a</sup> = 12801				

<sup>a</sup> NC: Total number of cells.

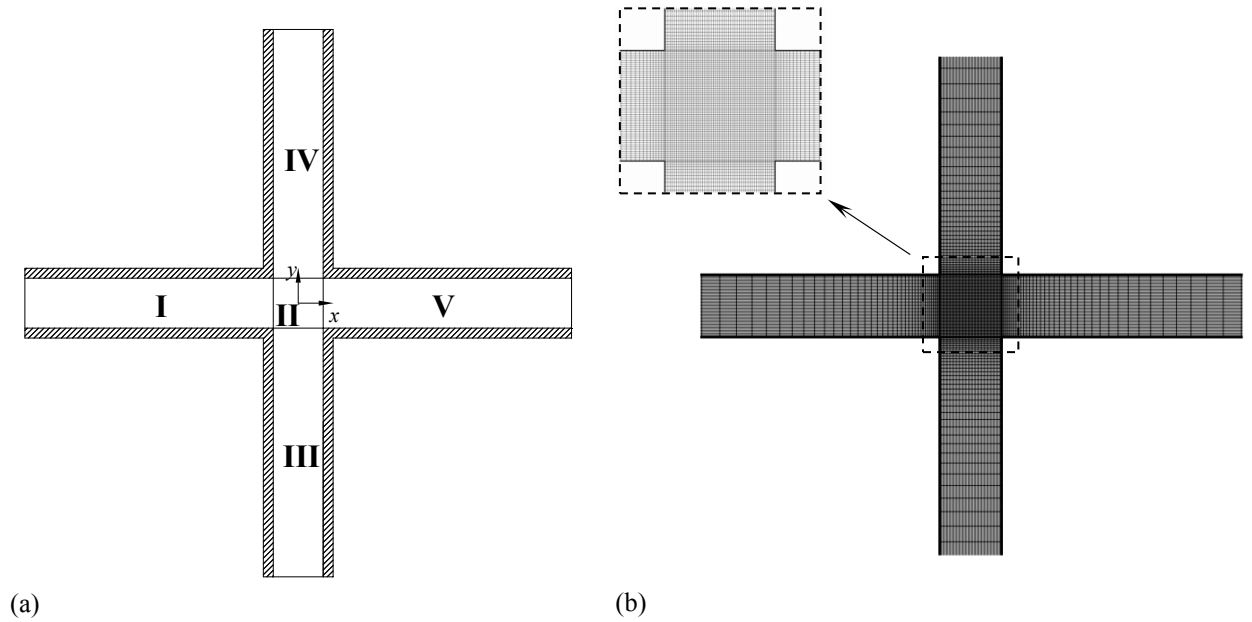


**Fig.3.** (a) Schematic representation of the blocks used to generate the mesh. (b) Zoomed view of mesh ( $-4 \leq x/d \leq 4$ ;  $-4 \leq y/d \leq 4$ ).

## 5 Results and discussion

Results of the computations are presented in three subsections: first, we analyze the effect of elasticity varying only the Deborah number and keeping the remaining parameters constant ( $L^2 = 100$  and  $\beta = 0.1$ ); second, we analyze the effect of solvent viscosity ratio for  $\beta = 0.05, 0.10$  and  $0.20$  ( $L^2 = 100$ ); and finally, we study the influence of extensibility parameter of the FENE-CR model for  $L^2 = 50, 100$  and  $200$  ( $\beta = 0.1$ ).

In this study we define a non-dimensional parameter  $DQ = (Q_2 - Q_1)/Q$  to quantify the degree of asymmetry of the flow [3]. The total flow rate supplied to each inlet channel  $Q = Q_1 + Q_2 = Ud$  is divided in two partial flow rates  $Q_1$  and  $Q_2$ , as illustrated in Fig. 2. For a symmetric flow  $Q_1 = Q_2 \Rightarrow DQ = 0$  and for an asymmetry flow  $Q_1 \neq Q_2 \Rightarrow DQ \neq 0$  (completely asymmetric flow  $\Rightarrow DQ = \pm 1$ ). Before presenting the predicted results we look at the effect of mesh refinement, using a more refined mesh with 101 cells across each channel, so with four times more cells than that of our base mesh detailed in Table 1 (NC = 50601 with  $\Delta x_{\min} \approx \Delta y_{\min} \approx 0.01d$ , as in the work of Poole *et al.* [3]. Figure 4 shows the bifurcation plot (Fig. 4(a)) and the velocity profile along the

central plane ( $y = 0$ ) (Fig. 4(b)) for a Deborah number of  $De = 0.40$ , on both the “coarse” mesh (51 cells) and the finer mesh (101 cells), at fixed base values of  $\beta = 0.1$  and  $L^2 = 100$ .

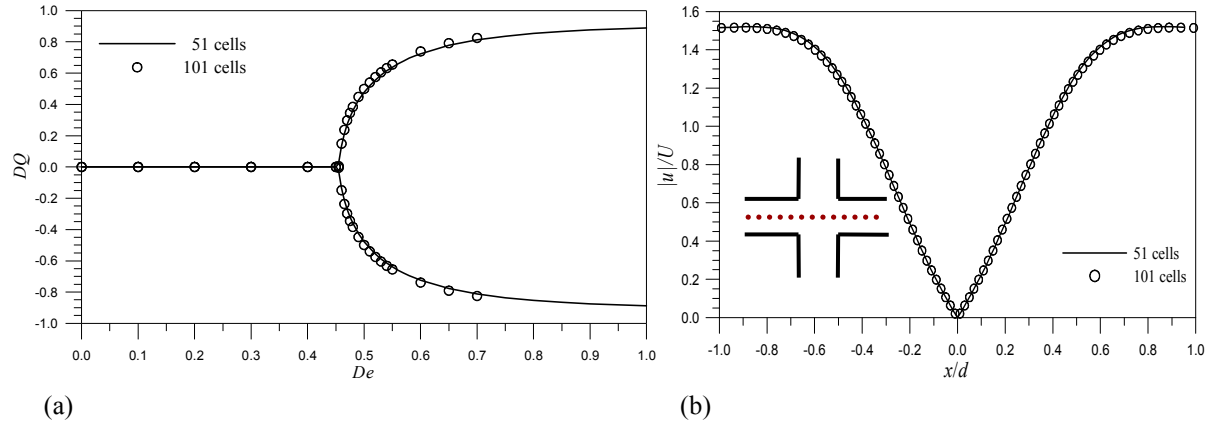


**Fig.4.** Effect of mesh refinement: (a) Variation of asymmetry parameter  $DQ$  with  $De$ ; (b) Velocity profile along the central plane ( $y = 0$ ) ( $De = 0.40$ ,  $L^2 = 100$  and  $\beta = 0.1$ ).

Clearly Fig. 4 reveals that the numerical results present a good level of agreement between the two meshes, thus justifying the use of the coarse mesh illustrated in Fig. 2(b) for the 2-D simulations in all remaining calculations.

### 5.1 Effect of Deborah number

The Deborah number is a dimensionless parameter used to measure the effect of elasticity of the fluid on the flow, which provides a relative measure of the magnitude of the elastic to viscous stress, as defined previously. In this case, we only modify the relaxation time  $\lambda$ , which represents a time constant of the material. Small Deborah numbers correspond to situations where in a flow the material has time to relax (and behaves in a viscous manner), while high Deborah numbers correspond to situations where the flowing material behaves rather elastically.

We start by presenting in Fig. 5 the predictions of the degree of asymmetry ( $DQ$ ) for Deborah numbers from 0.0 (Newtonian) to 1.0, at  $L^2 = 100$  and  $\beta = 0.1$ . The results of  $DQ$  vs  $De$  shown in Fig. 5 indicate a transition phenomena, with symmetric flow evolving to asymmetric flow, controlled by the critical Deborah number ( $De_{cr}$ ).

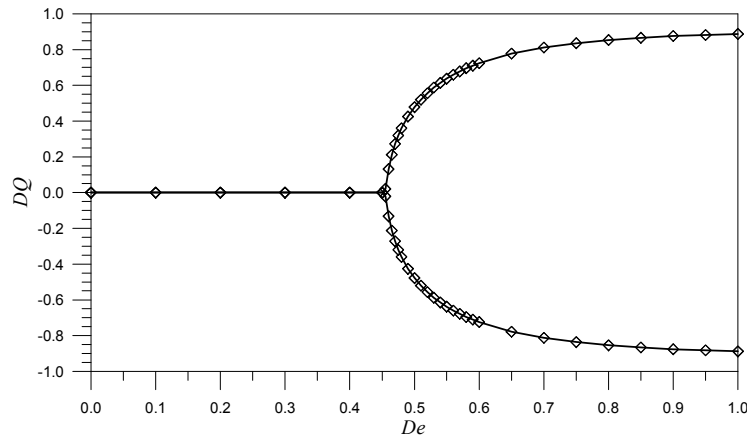


**Fig.5.** Variation of asymmetry parameter  $DQ$  with Deborah number ( $L^2 = 100$  and  $\beta = 0.1$ ).

It is seen from Fig. 5 that, for the Newtonian flow ( $De = 0$ ) and  $De \leq De_{cr}$ , the expected symmetry of the flow is confirmed but for Deborah numbers above a critical value (in this case  $De_{cr} = 0.46$ ) the flow becomes increasingly asymmetric but still steady, in agreement with the results reported by Arratia *et al.* [2] and Poole *et al.* [3].

In this geometry the asymmetry of the flow is triggered by elasticity, and since the Reynolds number in the present simulations is exactly zero it is demonstrated that the bifurcation is a purely-elastic phenomenon. Figure 6 presents the streamlines for increasing values of Deborah number, starting from  $De = 0.0$  (Newtonian), 0.4 (just before bifurcation), 0.46 (just after bifurcation) and 0.70, with  $L^2 = 100$  and  $\beta = 0.1$ . These steady-state plots of the flow pattern illustrate the sudden nature of the bifurcation, occurring at  $De_{cr} = 0.46$  for the set of parameters chosen, and the progressive evolution to an almost complete asymmetric configuration. It is emphasized that the image configuration of Fig. 6 (c,d), by rotating this about the  $x$ -axis by  $180^\circ$ , could occur as well, depending on the initial conditions and numerical parameters.

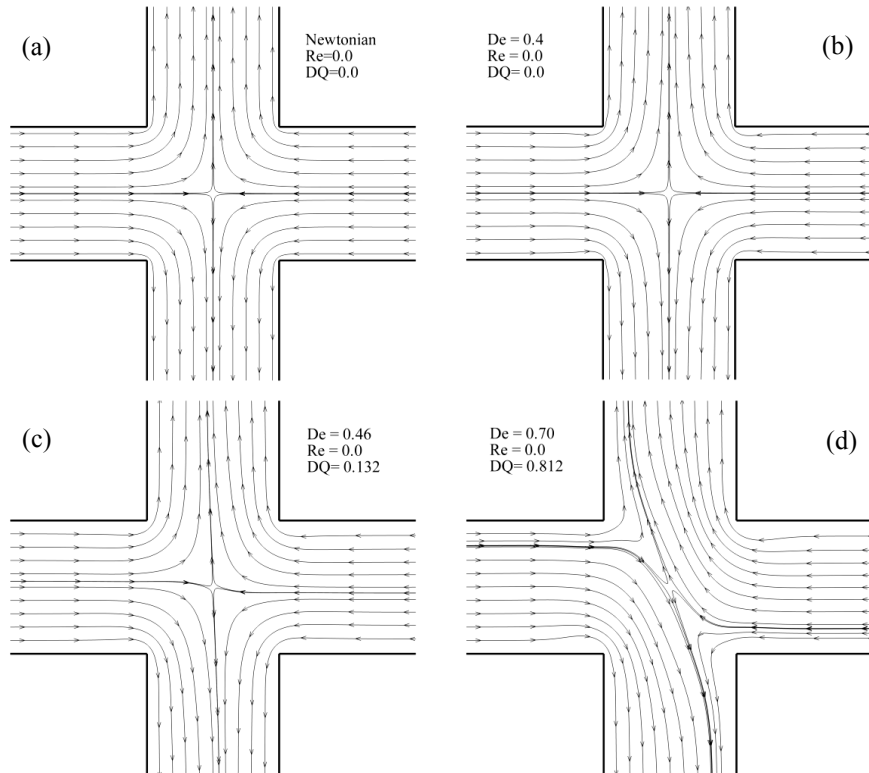


**Fig.6.** Predicted streamline plots for: (a)  $De = 0.0$  (Newtonian fluid); (b)  $De = 0.40$ ; (c)  $De = 0.46$ ; and (d)  $De = 0.70$  ( $L^2 = 100$  and  $\beta = 0.1$ ).

## 5.2 Effect of concentration, $\beta$

The  $\beta$  parameter measures the ratio of solvent shear viscosity to total shear viscosity and provides a measure of polymer concentration. For the present study we used  $\beta = 0.05, 0.10$  and  $0.20$ , at fixed  $L^2 = 100$ , and the results of the present parametric study, in terms of the degree of asymmetry ( $DQ$ ), are provided in Table 2 and qualitatively illustrated in Fig. 7.

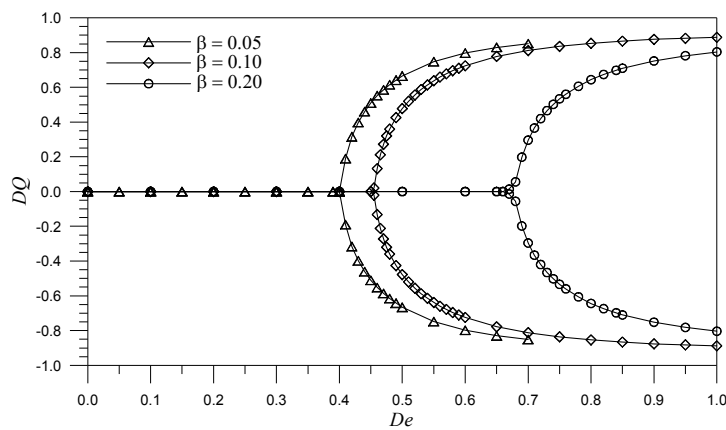


**Fig.7.** Variation of asymmetry parameter  $DQ$  with  $De$  number: Influence of solvent viscosity ratio  $\beta$  ( $L^2 = 100$ ).

**Table 2.** Bifurcation data ( $L^2 = 100$ ).

$\beta = 0.05$		$\beta = 0.10$		$\beta = 0.20$	
$De$	$DQ$	$De$	$DQ$	$De$	$DQ$
0.00	0.000	0.00	0.000	0.00	0.000
0.20	0.000	0.20	0.000	0.20	0.000
0.40	0.000	0.40	0.000	0.40	0.000
<b>0.41</b>	<b>0.190</b>	0.45	0.000	0.50	0.000
0.42	0.316	<b>0.46</b>	<b>0.132</b>	0.60	0.000
0.43	0.398	0.47	0.272	0.65	0.000
0.44	0.460	0.48	0.360	0.67	0.000
0.45	0.510	0.49	0.426	<b>0.68</b>	<b>0.056</b>
0.46	0.552	0.50	0.478	0.69	0.198
0.47	0.586	0.51	0.520	0.70	0.296
0.48	0.616	0.52	0.556	0.71	0.366
0.49	0.642	0.53	0.588	0.72	0.420
0.50	0.666	0.54	0.614	0.73	0.446
0.55	0.748	0.55	0.638	0.74	0.502
0.60	0.798	0.60	0.724	0.75	0.534
0.65	0.830	0.70	0.812	0.80	0.644
0.70	0.852	0.80	0.854	0.85	0.710
---	---	0.90	0.876	0.90	0.752
---	---	1.00	0.888	1.00	0.804
$De_{cr} \approx 0.41$		$De_{cr} \approx 0.46$		$De_{cr} \approx 0.68$	

From Fig. 7 it is worth noting that increasing  $\beta$  leads to a delay of the critical bifurcation point. Since  $1 - \beta$  is inversely proportional to the polymer concentration, then this outcome maybe interpreted as resulting from larger fluid elasticity. A compilation of the predicted results for the critical Deborah number gives the following data:

- $\beta = 0.00$ :  $De_{cr} = 0.31$  ( $L^2 = \infty$ ) [3];
- $\beta = 0.05$ :  $De_{cr} = 0.41$
- $\beta = 0.10$ :  $De_{cr} = 0.46$
- $\beta = 0.20$ :  $De_{cr} = 0.68$
- $\beta \rightarrow 1.00$ :  $De_{cr} \rightarrow \infty$ .

### 5.3 Influence of extensibility, $L^2$

The  $L^2$  parameter is a measure of extensional effects and represents the square of the ratio between the maximum and the equilibrium lengths of the polymer molecules. When  $L^2$  tends to infinity the function  $f$  tends to unity (cf. Eq. (5)), and the constitutive equation (4) reduces to the well-known upper-convected Maxwell or Oldroyd-B models which were applied in the numerical work of Poole *et al.* [3]. Here, we decided to increase  $L^2$  in the range 50, 100 and 200 (at fixed  $\beta = 0.1$ ), and the results are provided in Table 3 and plotted in Fig. 8 ( $\beta = 0.1$ ).

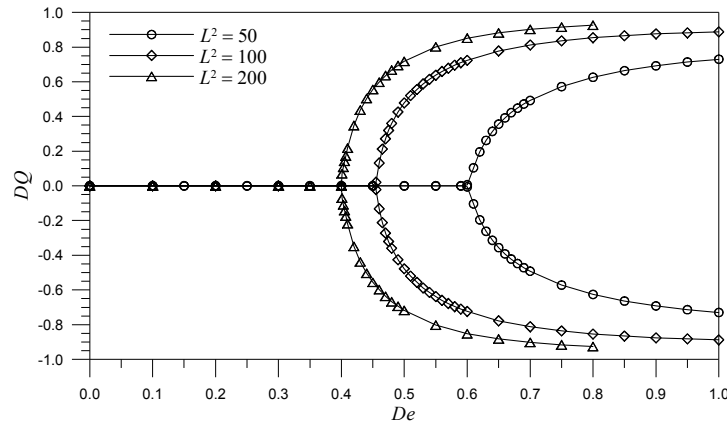


**Fig.8.** Variation of asymmetry parameter  $DQ$  with  $De$  number:  
Influence of extensibility parameter  $L^2$  ( $\beta = 0.1$ ).

**Table 3.** Bifurcation data ( $\beta = 0.1$ ).

$L^2 = 50$		$L^2 = 100$		$L^2 = 200$	
$De$	$DQ$	$De$	$DQ$	$De$	$DQ$
0.00	0.000	0.00	0.000	0.00	0.000
0.20	0.000	0.20	0.000	0.20	0.000
0.40	0.000	0.40	0.000	0.40	0.000
0.50	0.000	0.45	0.000	<b>0.41</b>	<b>0.218</b>
0.60	0.006	<b>0.46</b>	<b>0.132</b>	0.42	0.348
<b>0.61</b>	<b>0.104</b>	0.47	0.272	0.43	0.438
0.62	0.196	0.48	0.360	0.44	0.504
0.63	0.262	0.49	0.426	0.45	0.556
0.64	0.314	0.50	0.478	0.46	0.598
0.65	0.356	0.51	0.520	0.47	0.636
0.66	0.392	0.52	0.556	0.48	0.668
0.67	0.422	0.53	0.588	0.49	0.694
0.68	0.448	0.54	0.614	0.50	0.718
0.69	0.472	0.55	0.638	0.55	0.802
0.70	0.492	0.60	0.724	0.60	0.852
0.75	0.572	0.70	0.812	0.65	0.882
0.80	0.626	0.80	0.854	0.70	0.902
0.90	0.692	0.90	0.876	0.75	0.916
1.00	0.730	1.00	0.888	0.80	0.926
<b><math>De_{cr} \approx 0.61</math></b>		<b><math>De_{cr} \approx 0.46</math></b>		<b><math>De_{cr} \approx 0.41</math></b>	

Our results show that an increase in the extensibility parameter ( $L^2$ ) of the FENE-CR model tends to accentuate the bifurcation phenomenon upon the base flow and to shift the occurrence of the transition point to asymmetry to lower Deborah numbers.

Figure 9 shows the streamline plots near the critical points of transition to asymmetry, for  $L^2 = 50, 100$  and  $200$  ( $\beta = 0.1$ ). As  $L^2$  increases the critical  $De$  values are lowered. Therefore, from Sections 5.2 and 5.3, we see that the instability leading to the flow asymmetry in the cross-slot is enhanced as elasticity is increased through both polymer concentration (inversely proportional to  $\beta$ ) and extensibility (directly proportional to  $L^2$ ). Both these factors lower the critical Deborah number.



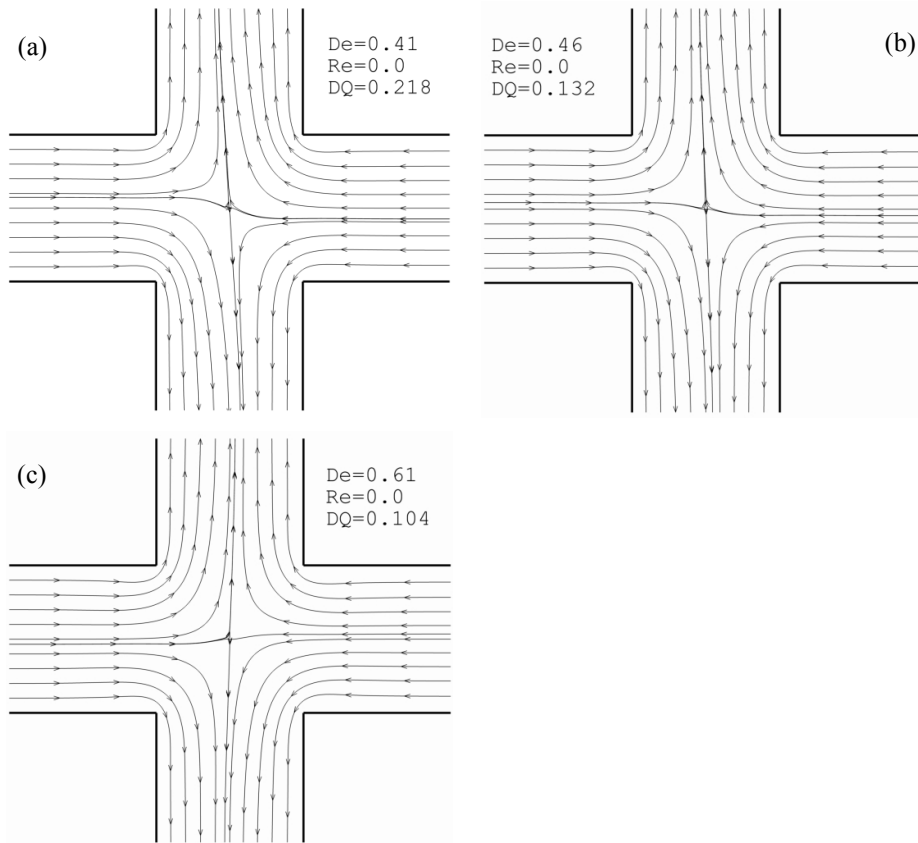


Fig.9. Predicted streamline plots for: (a)  $L^2 = 200$ ; (b)  $L^2 = 100$ ; and (c)  $L^2 = 50$  ( $\beta = 0.1$ ).

## 6 Conclusions

Computations have been performed using a finite-volume method for the inertia less ( $Re = 0$ ) flow of a viscoelastic FENE-CR fluid in a planar cross-slot geometry. Steady-state results were obtained in the range  $De = 0 - 1.0$  for the full domain. A comprehensive parametric study has been conducted leading to the following conclusions regarding the separate effect of each individual parameter analyzed.

- Elasticity was seen to directly drive the instability: for  $De$  values lower than a critical Deborah number the flow remains symmetric and stable, while for values above  $De_{cr}$  the flow becomes asymmetric and stable. This parameter fully defines the transition point between the symmetric and asymmetric state. However,  $De_{cr}$  depends on both  $\beta$  (polymer concentration) and  $L^2$  (extensible elasticity).
- Polymer concentration, through the parameter  $\beta$ , was seen to have a strong effect: for  $\beta = 0.20$ , at  $L^2 = 100$ , the flow was symmetric and steady up to  $De_{cr} \approx 0.67$ , but if  $\beta$  was decreased to 0.10 (increasing polymer concentration) the asymmetry phenomenon appears at lower  $De$  (see Fig. 7).
- Extensibility parameter  $L^2$ ; this parameter controls the extensional viscosity and the critical Deborah number decreases with increasing values of the FENE-CR extensibility parameter, i.e. for  $L^2 = 100 \rightarrow De_{cr} \approx 0.46$  and  $L^2 = 200 \rightarrow De_{cr} \approx 0.41$ , at a fixed  $\beta = 0.1$  (see Fig. 8).

## Acknowledgments

The authors would like to acknowledge the financial support from Fundação para a Ciência e a Tecnologia (FCT, Portugal) under projects PTDC/EME-MFE/70186/2006, PTDC/EQU-FTT/71800/2006 and the Ph.D. scholarship SFRH/BD/22644/2005 (G.N. Rocha).

## References

1. R.G. Larson, E.S.G. Shaqfeh and S.J. Muller, A purely elastic instability in Taylor-Couette flow, *J. Fluid Mech.*, 218, 573-600, 1990.
2. P.E. Arratia, C.C. Thomas, J.D. Diorio and J.P. Gollub, Elastic instabilities of polymer solutions in extensional flows, *Physical Review Letters*, 96 (14), 144502(4), 2006.
3. R.J. Poole, M.A. Alves and P.J. Oliveira, Purely-elastic flow asymmetries, *Physical Review Letters*, 99(16), 164503(4), 2007.

4. R.B. Bird, C.F. Curtiss, R.C. Armstrong and O. Hassager, *Dynamics of Polymeric Liquids, Vol. 2: Kinetic Theory*, Wiley, New York, 1987.
5. M.D. Chilcott and J.M. Rallison, Creeping flow of dilute polymer solutions past cylinders and spheres, *J. Non-Newtonian Fluid Mech.*, 29, 381-432, 1988.
6. C.M. Rhie and W.L. Chow, Numerical study of the turbulent flow past an airfoil with trailing edge separation, *AIAA Journal*, 21, 1525-1532, 1983.
7. P.J. Oliveira, F.T. Pinho and G.A. Pinto, Numerical simulation of non-linear elastic flows with a general collocated finite-volume method, *J. Non-Newtonian Fluid Mech.*, 79, 1-43, 1998.
8. M.A. Alves, P.J. Oliveira and F.T. Pinho, A convergent and universally bounded interpolation scheme for the treatment of advection, *Int. J. Numer. Mech. Fluids*, 41, 47-75, 2003.
9. P.K. Kosla and S.G. Rubin, A diagonally dominant second-order accurate implicit scheme, *Computers and Fluids*, 2, 207-209, 1974.
10. J.P. Van Doormal and G.D. Raithby, Enhancements of the SIMPLE method for predicting incompressible fluid flows, *Numerical Heat Transfer*, 7, 147-163, 1984.
11. S.V. Patankar and D.B. Spalding, A calculation procedure for heat, mass, and momentum transfer in three-dimensional parabolic flows, *Int. J. Heat and Mass Transfer*, 15, 1787-1806, 1972.